Langmuir
The ACS Journal of Surfaces and Colloids

JANUARY 5, 1999
VOLUME 15, NUMBER 1

Letters

Hydrogen-Induced Deformations of Metals Followed by in Situ Scanning Tunneling Microscopy. Palladium Electrolytic Hydrogen Charging and Discharging in Alkaline Solution

G. Andreasen, A. Visintin, R. C. Salvarezza, W. E. Triaca, and A. J. Arvia*

Instituto de Investigaciones Fisicoquímicas Teóricas y Aplicadas (INIFTA), Casilla de Correo 16, Sucursal 4, (1900) La Plata, Argentina

Received June 1, 1998. In Final Form: October 30, 1998

In situ scanning tunneling microscopy measurements of Pd single-crystal domains during hydrogen charging/discharging cycles in 0.25 M KOH at 298 K allowed us to follow deformations produced by the Pd ⇔ β(H−Pd) phase transition in real time. The stress produced by this transition leads to elastic deformations involving reversible volume changes and plastic deformations resulting in one- or two-atom high slip lines and slip bands. These results demonstrate the capability of nanoscopies to investigate solid deformations on the nanometer scale in different environments, discriminate different types of deformations, and distinguish possible additional steps that are involved in the dynamics of solids.

The deformation of a stressed crystal implies essentially elastic-, inelastic- and plastic-type deformations that are often simultaneously present.[1] Elastic deformations are instantaneous and reversible; i.e., they disappear when the stress is removed. They involve changes in the volume and shape of the solid. Inelastic deformations exhibit characteristics similar to those of elastic deformations although they are retarded. Plastic deformations appear when the shear stress applied to the solid exceeds the elasticity limit. In contrast to elastic and inelastic deformations, plastic deformations are irreversible and produce changes in the morphology of the solid but not in its volume, the crystal lattice characteristics remaining unchanged. Plastic deformations produce localized slip lines and bands from dislocation motions.

Mechanical deformation of metals by cathodically produced hydrogen charging has been extensively studied in relation to hydrogen embrittlement,[2] the use of different metals for hydrogen storage,[3] and cold fusion controversial procedure for energy conversion. Among all metals, Pd is probably the most studied due to its ability to occlude hydrogen.[4] The cathodic deposition of hydrogen on a number of metals involves complex hydrogen−metal interactions accompanying the hydrogen evolution reaction.[5] These complex interactions result in various processes that are specific to the permeability, occlusive properties of the metal electrode, and environment conductivity. Typical examples are the formation of hydrides for Pd, hydrogen embrittlement for Fe and other metals, and the deformation produced in the hydrogen-

(1) Bordoni, P. G. In *Mechanical Properties and Behaviour of Solids: Plastic Instabilities*; Balakrishnan, V., Bottani, C. E., Eds.; World Scientific: Singapore, 1986; p 110.

(2) Subramanian, P. G. In *Comprehensive Treatise of Electrochemistry*; Bockris, J. O'M., Conway, B. E., Yeager, E., White, R. E., Eds.; Plenum Press: New York, 1981; Vol. 4, Chapter 8, p 411.

(3) Smith, D. P. *Hydrogen in Metals*; The University of Chicago Press: Chicago, IL, 1948.

(4) Lewis, F. A. *The Hydrogen Palladium System*; Academic Press: London, 1967.

(5) Salvarezza, R. C.; Montemayor, M. C.; Fatas, E.; Arvia, A. J. *J. Electroanal. Chem.* **1991**, *313,* 291.

10.1021/la980633f CCC: $18.00
Published on Web 12/15/1998

containing environment that in turn changes the permeability of metals themselves.[2,3]

Three possible mechanisms have been advanced to explain hydrogen embrittlement, namely, the stress-induced hydride formation and cleavage mechanism,[6−9] the hydrogen-enhanced localized plasticity mechanism,[10−14] and the hydrogen-induced decohesion mechanism.[15,16] The first mechanism has been established for those metal−hydrogen systems in which either stable hydrides are formed or hydrides can be stabilized by the application of a stress field. The mechanism of hydrogen-enhanced localized plasticity is based on the fact that in a range of temperature and strain rates, the presence of hydrogen in solid solution decreases the barriers to dislocation motion, thereby increasing the amount of deformation that occurs in a localized region adjacent to the fracture surface. The fracture process has been considered as a highly localized plastic failure process rather than as hydrogen embrittlement. The third mechanism that is applicable to non-hydride-forming systems implies that the atomic bonding at the crack tip is weakened by the presence of hydrogen in the solid solution.[15]

The flow and fracture of materials at high resolution are usually studied employing different techniques such as synchrotron X-ray topography, transmission electron microscopy, scanning electron microscopy, acoustic emission, and current noise. These methods mainly provide average information about the dynamic behavior of stressed solids. More recently, in situ transmission electron microscopy has been used to observe fracture processes in real time and high spatial resolution.[17]

In this Letter, in situ scanning tunneling microscopy (STM) is used to follow the behavior of Pd single-crystal domains in real time under electrolytic hydrogen charging/discharging cycles in 0.25 M KOH at 298 K. Our results for this system show that elastic and plastic deformations are related to the Pd ⇔ β-HPd phase changes undergoing during the electrolytic hydrogen charging/discharging cycles. Recently, STM has been used to investigate the elastic deformation of V−Ti−Ni multiphase alloy electrodes under hydrogen charging.[18] Our results demonstrate that nanoscopies can also be used to study plastic deformation of solids and crack opening on the nanometer scale in real time.

Experiments were run in aqueous 0.25 M KOH at 298 K using a KEL-F-made electrochemical cell as part of a Nanoscope III scanning tunneling microscope for in situ STM imaging. Polycrystalline mirror-polished Pd plates annealed at 900−1000 K under purified nitrogen for 5 min were employed as working electrodes. Thus, the working electrode consisted of a collection of 30−50 μm average size single crystals separated by 2 μm average width boundaries. Single crystal domains could be selected for STM imaging. A large Pt counter electrode and a Pd/H_2 reference electrode (E_r) were employed in the cell. Solutions were prepared from analytical grade chemicals and triply distilled water. They were bubbled with purified nitrogen for 2 h before carrying out the experiments. STM imaging was made using a Nanoscope III instrument (Santa Barbara, CA) operating under the topographic mode. Pt−Ir nanotips Apiezon covered to decrease the faradaic currents were employed. Typical tip voltage E_{tip} = 0.6 V (vs Pd/H_2 reference electrode) and tunneling current i_t = 10 nA were used. Ex situ AFM images were also obtained with Si_3N_4 tips using typical forces in the range 10−30 nN.

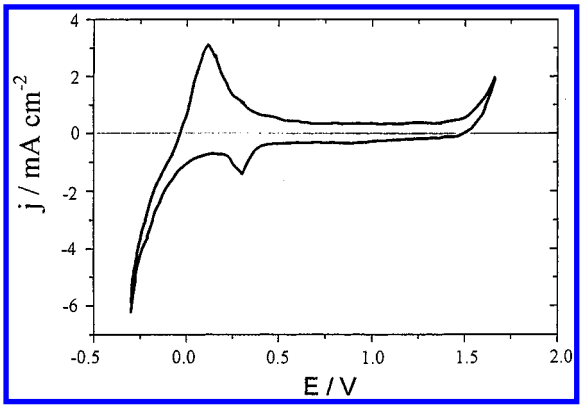

Figure 1. Current density (j) vs applied potential (E) profile recorded at 0.02 V/s for Pd in aqueous 0.25 M KOH at 298 K.

A typical current density (j) vs applied potential (E) profile, recorded at 0.02 V/s (Figure 1) for Pd in aqueous 0.25 M KOH at 298 K starting by shifting the potential negatively from 0.2 to −0.30 V, shows an exponential increase in the cathodic current density (j_c) for $E < 0$ V due to the discharge of hydrogen ions. The first step of the overall process is the electroadsorption of H from the discharge of water according to

$$Pd + H_2O + e^- = Pd(H)_{ad} + OH^- \qquad (1)$$

The following steps depend on the value of j_c. In principle, two competing steps can be distinguished, hydrogen absorption by diffusion of H atoms into bulk Pd (hydrogen occlusion)

$$Pd(H)_{ad} = (PdH)_{ab} \qquad (2a)$$

and molecular hydrogen formation according to

$$Pd(H)_{ad} + Pd(H)_{ad} = H_2(g) + 2\ Pd \qquad (2b)$$

Step 1 undergoes close to conditions of equilibrium and implies a relatively low degree of surface coverage.[19] Step 2a involves the formation of PdH alloys. Step 2b, which corresponds to the hydrogen evolution reaction on Pd, is favored at high values of j_c, in particular when the hydrogen saturation of Pd has been attained.

(6) Westlake, D. G. *Trans. ASM* **1969,** *62,* 1000.
(7) Birnbaum, H. K.; Grossbeck M.; Gahr, S. In *Hydrogen in Metals*; Bernstein, M., Thompson A. W., Eds.; ASM: Metals Park, OH, 1973; p 303.
(8) Gahr, S.; Grossbeck, M.; Birnbaum, H. K. *Acta Metall.* **1977**, *25,* 1775.
(9) Shih, D.; Robertson, I. M.; Birnbaum, H. K. *Acta Metall.* **1988**, *36,* 111.
(10) Beachem, C. D. *Metall. Trans.* **1972**, *3,* 437.
(11) Birnbaum, H. K. In *Environment-induced Cracking of Metals*; Gangloff, R. P., Ives, M. B., Eds.; NACE: Houston, 1988; p 21.
(12) Myers, S. M.; Baskes, M. I.; Birnbaum H. K.; Corbett, J. W.; Deleo, G. G.; Estreicher, S. K.; Haller, E. E.; Jena, P.; Johnson, N. M.; Kirchheim, R.; Pearton, S. J.; Stavola, M. J. *Rev. Mod. Phys.* **1992**, *64,* 559.
(13) Sirois, E.; Sofronis, P.; Birnbaum, H. K. In *Fundamental Aspects of Stress Corrosion Cracking*; Bruemmer, S. M., Ed.; The Minerals, Metals and Material Sciences: New York, 1992; p 173.
(14) Birnbaum, H. K., Moody, M., Thompson, A. W., Eds. *Hydrogen Effects on Material Behavior*; The Minerals, Metals and Material Sciences: New York, 1990; p 639.
(15) Birnbaum, H. K.; Sofronis, P. *Mater. Sci. Eng. A* **1994**, *176,* 191.
(16) Oriani, R. A.; Josephic, P. H. *Acta Metall.* **1965**, *22,* 1065.
(17) Tabata, T.; Birnbaum, H. K. *Scr. Metall.* **1984**, *18,* 231; **1984**, *187,* 947.
(18) Kuriyama, N.; Chartouni, D.; Tsukahara, M.; Takahashi, K.; Takeshita, H. T.; Tanaka, H.; Schlapbach, L.; Sakai, T.; Uehara, I. *Electrochem. Solid-State Lett.* **1998**, *1,* 37.
(19) Mengoli, G.; Bernardini, M.; Fabrizio, M.; Manduchi, C.; Zannoni, G. *J. Electroanal. Chem.* **1996**, *403,* 143.

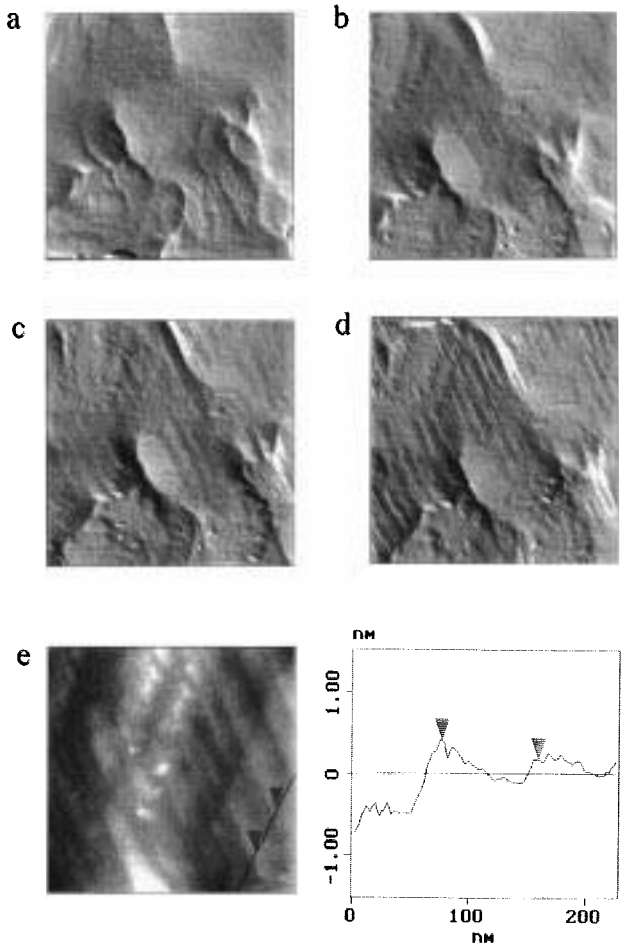

Figure 2. Sequential 1000 × 1000 nm² in situ STM images (top view, high pass filtered) of a Pd(111) domain in 0.25 M KOH at 298 K. (a) At $j = 0$ no topographic change can be observed. At $j_c = 34$ mA/cm² the progressive formation of slip lines during hydrogen charging can be observed. Hydrogen charging time (b) $t = 768$ s; (c) $t = 1140$ s; (d) $t = 1870$ s. (e) Cross section showing monatomic and diatomic high slip lines (see arrows).

The dynamic polarization curve subsequently recorded from −0.30 V backward shows first a cathodic current related to the hydrogen ion discharge, and from ca. 0 V upward the appearance of a large anodic peak at 0.13 V that is related to hydrogen stripping from Pd. In the range 0.5 V < E < 1.3 V the formation of PdO takes place. For E > 1.3 V the increase in the anodic current due to the oxygen evolution reaction can be observed. The reverse potential scan run from 1.7 to 0.2 V shows the cathodic peak related to PdO electroreduction at 0.35 V.

The initial stages of hydrogen occlusion in Pd involve the formation of the α-HPd alloy with a slight increase in the lattice constant from $d = 0.3883$ nm for Pd to $d = 0.3894$ for α-HPd.[4] At more advanced hydrogen absorption stages, when the stoichiometry 0.6 H/Pd is reached, the formation of β-HPd alloy with $d = 0.4018$ nm takes place, i.e., about 3% increase in the lattice constant is produced.[4]

In situ STM images of a smooth domain taken for 5 min on a large Pd single crystal at a null net current ($j = 0$) were first obtained (Figure 2a). In this way drift effects could be diminished. Then, the tip was placed at a position (x,y,z) and the piezo shift in the z-direction to maintain the tip−sample distance constant, and the electrode potential (E) were simultaneously determined (Figure 3). For $j = 0$, changes neither in the Pd topography nor in the z-position of the piezo could be observed (Figure 3 region A). Afterward, E was adjusted to start the hydrogen charging of Pd at $j_c = 34$ mA cm⁻², a value sufficiently high to form simultaneously the β-HPd phase and molecular hydrogen on Pd.[20] Finally, the hydrogen charging process produced a negative shift to −0.27 V and, simultaneously, the retraction of the piezo at a constant rate of about 2.6 nm/s to keep the tip−Pd surface distance constant (Figure 3, region B). This retraction of the piezo was caused by the increase in the volume of the Pd electrode during hydrogen charging.

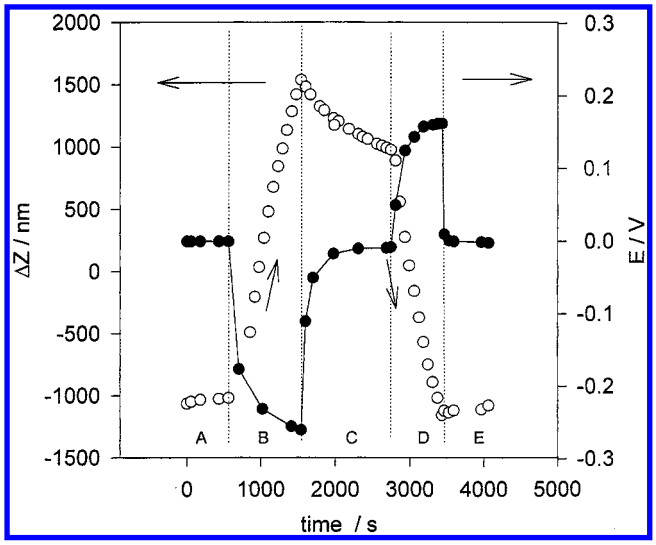

Figure 3. Piezoelectric displacement (Δz) vs t and E vs t plots. Regions A, C, and E correspond to $j = 0$. Region B corresponds to $j_c = 34$ mA/cm². Region D corresponds to $j_a = 34$ mA/cm².

After 25 min of cathodic hydrogen charging, the circuit was opened for a few seconds for Pd self-discharging. This process produced the displacement of E from −0.27 to 0 V and caused the piezo to move in at a rate lower than that observed in the charging process (Figure 3, region C). Afterward, E was adjusted to $E = 0.2$ V to reach the anodic current density, $j_a = 34$ mA cm⁻² for absorbed hydrogen removal at a higher rate. In this case, the piezoelectric (Figure 3, region D) moved in faster than under the open circuit condition, the rate of piezoelectric displacement being similar to that observed for hydrogen charging. Finally, at the end of the hydrogen discharge as indicated by the change of Δz, when the circuit was opened E decreased to 0 V and the piezo returned to its initial z-position (Figure 3, region E).

For both hydrogen charging and discharging cycles, the maximum piezoelectric displacement is 2.6 × 10⁻⁴ cm. Assuming that the diffusion coefficient of hydrogen in β-HPd is $D = 1 \times 10^{-7}$ cm² s⁻¹,[4,5] the penetration depth (l) of hydrogen into the bulk metal after $t = 1500$ s is $l = 0.017$ cm. As there is a 3% expansion in going from Pd to β-HPd,[4] for a Pd cube of side $l = 0.017$ cm the length increase results in $\Delta l = 5 \times 10^{-4}$ cm. This value of Δl is just twice the value determined for each charging/discharging cycle from the piezo displacement in the z-direction. Therefore, from this reversible behavior and the magnitude of the piezoelectric displacement it can be concluded that electrochemical processes are related to the initial elastic deformation of Pd caused by hydride formation. However, the above estimation assumes isotropic expansion while adjacent crystals and crystal boundaries could limit expansion to one direction. However, if this were the case, it would result in $\Delta l \approx 15 \times$

(20) Pfeiffer, B.; Thyssen, A.; Schultze, J. W. *J. Electroanal. Chem.* **1989**, *260,* 393.

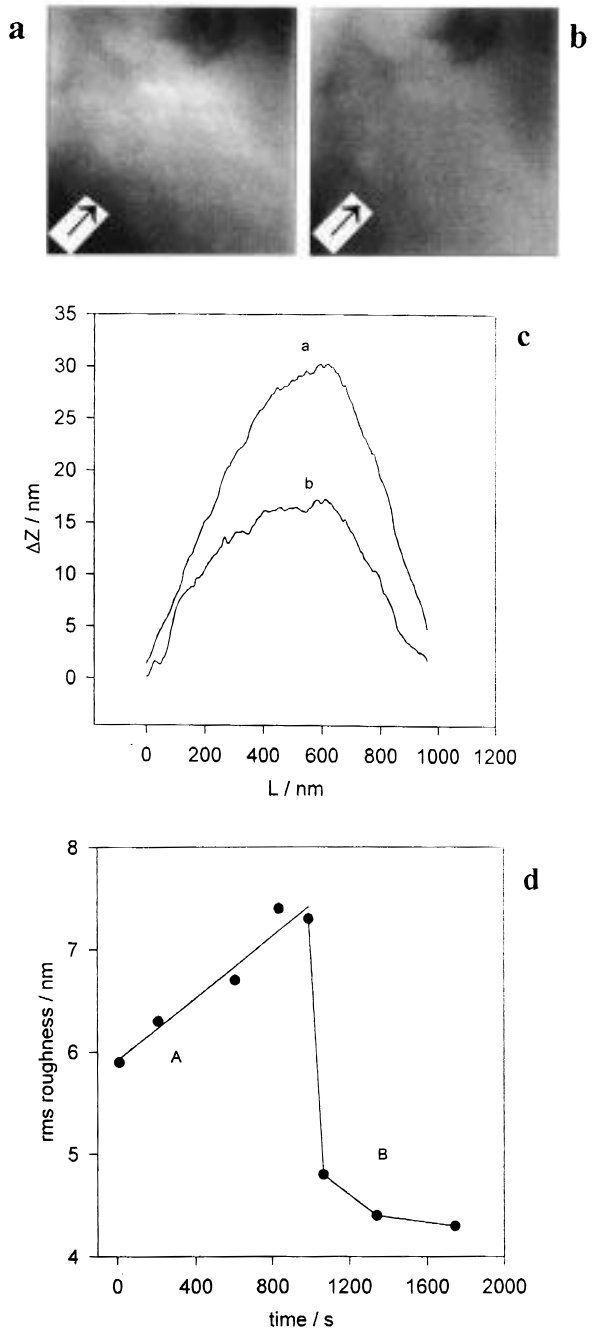

Figure 4. Sequential 690 × 690 nm^2 in situ STM images (top view) of a Pd(111) domain in 0.25 M KOH at 298 K. (a) $j_c = 34$ mA/cm^2; $t = 980$ s. (b) Image taken immediately after opening the circuit ($j = 0$); $t = 1060$ s. (c) Cross section of images (a) and (b) taken in the directions indicated in these images, showing the relative decrease in Δz due to the loss of hydrogen. (d) The rms roughness vs t plot. Regions A and B correspond to images resulting from hydrogen charging and hydrogen self-discharging, respectively.

10^{-4} cm, a value greater than that resulting from the piezo displacement. Therefore, at this hydrogen charging stage an isotropic expansion seems to take place.

The sequential in situ STM images (Figure 4a,b) taken along the self-discharging process (open circuit) and their cross sections (Figure 4c,d) show remarkable changes in the topography of hydrogen-charged Pd electrodes. It is evident that the maximum height difference from the cross sections decreases from 31 nm for $j_c = 34$ mA cm^{-2} to 20 nm for $j = 0$. Accordingly, the root-mean-square roughness diminishes from 7 to 4.5 nm, respectively (Figure 4c), due to the loss of a small amount of hydrogen occluded in Pd even during self-discharging. It should be noted that this interesting conclusion results only from raw imaging data as either plane removal or flatten filtering eliminates volume changes produced during elastic deformations. Otherwise, filtering is required for the clear observations of topographic changes at the Pd surface caused by plastic deformations.

Sequential in situ STM images (Figure 2b–d) of a Pd single-crystal domain under hydrogen charging at $j = 34$ mA cm^{-2} show the progressive formation of monatomic or diatomic high steps (Figure 2e and cross section), which corresponds to slip lines intersecting at 60° angles, as should be expected from a Pd(111) surface. As the charging process takes place, the appearance of slip lines reduces the terrace width to 50 nm. Furthermore, the number of slip lines (N) at a given charging time estimated from STM images fulfills a linear N vs t plot with the slope $v = 10^6$ cm^{-2} s^{-1}, which represents the slip line generation rate. Slip lines result from the intersection of dislocations emerging at the Pd surface that relieve the stress caused by the Pd ⇒ β-HPd phase change. Slip bands 300–600 nm in height produced after charging the Pd electrode for 120 min are also clearly observed at a lower resolution ex situ AFM imaging (Figure 5a,b). These plastic deformations occur on the β-HPd phase formed near the surface during the charging process. Hydrogen-enhanced localized plasticity of dislocations has been observed within crystals and at grain boundaries.[15] Therefore, results from this work fit into the two most likely mechanisms for hydrogen embrittlement on hydride-forming systems. Finally, during hydrogen charging, crack opening at the Pd single-crystal surface can be shown in real time (Figure 6a,b).

Reversible phase selective potentiostatic cathodic hydrogenation of a V–Ti–Ni-based multiphase alloy has been recently imaged by in situ STM.[18] In this case neither plastic deformation nor crack opening has been observed, that is, the behavior of this alloy differs from our results from polycrystalline Pd. This difference would result from both the nature of the materials and, presumably, a smaller amount of hydrogen charged in the V–Ti–Ni-based multiphase alloy.

It should be noted that under conditions of equilibrium the stress (σ) related to the Pd ⇒ β-HPd phase change can be estimated from the following equation for the fugacity (f)[2]

$$f = \exp(-2\eta_c F/RT) \qquad (3)$$

η_c being the cathodic overvoltage defined as $\eta_c = E - E_r$, F the Faraday constant, R the universal gas constant, and T the temperature. Thus, for $\eta_c = -0.3$ V (Figure 3a), eq 3 yields $f = 10^{10}$,[2] a value that corresponds to $\sigma \approx 2$ Gpa. This value of σ is already about one order of magnitude greater than the tensile strength of the material.[21] Therefore, far from conditions of equilibrium for $j_c = 34$ mA cm^{-2} the Pd ⇒ β-HPd phase change produces a severe strain with plastic deformations that results in rift formation and rift opening, increasing then its occlusive capacity. Accordingly, the appearance of a severe strain explains the damage of the Pd single-crystal domain observed during the hydrogen charging runs. The greatest effect of hydrogen appears at crack tips, where hydrogen entry is facilitated either by slip processes or by the increase in the local hydrogen concentration by the effect of stress on the chemical potential of solute hydrogen.

(21) Lee, J. A.; Maxwell, H. L.; Fetter, E. C.; Dunkle, H. H. In *Chemical Engineers' Handbook* 3rd ed., Perry, J. H., Ed.; The American Institute of Chemical Engineers, McGraw-Hill: New York, 1949; Sect. 21, p 1543.

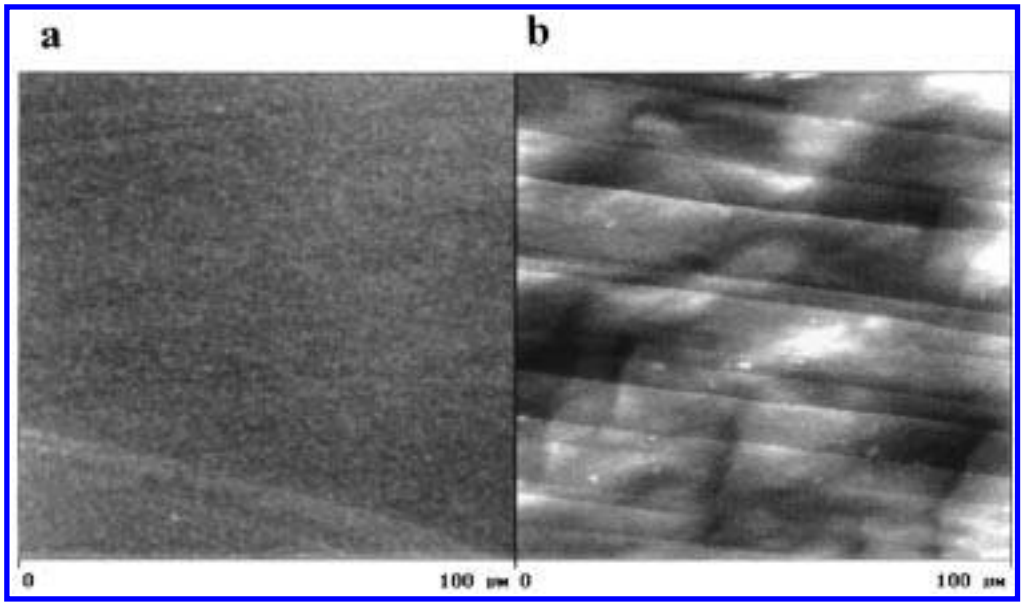

Figure 5. 100 × 100 μm^2 ex situ AFM images (top view) of a Pd(111) domain before (a) and after hydrogen charging for $t = 7200$ s (b) in 0.25 M KOH at 298 K. Slip band formation can be observed after hydrogen charging.

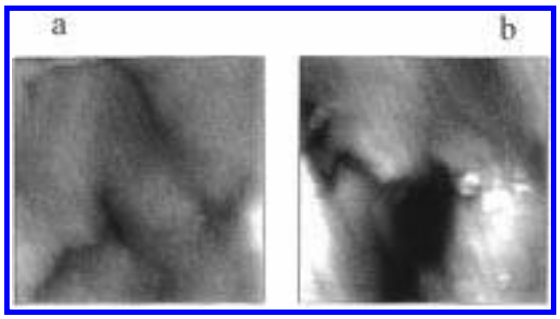

Figure 6. Sequential 1000 × 1000 nm^2 in situ STM images (top view, high pass filtered) of a Pd(111) domain during hydrogen charging in 0.25 M KOH at $j_c = 34$ mA/cm^2 and 298 K, for $t = 2000$ s (a) and $t = 2200$ s (b). Crack opening can be observed in (b).

Therefore, the high value of σ supports the rift theory of hydrogen occlusion in Pd.[3] It should also be noted that during HPd dealloying, the contraction resulting from the β-HPd ⇒ Pd phase change produces severe deformations enlarging rifts existing at the β-HPd phase itself, which remain in both the α-HPd intermediate phase and Pd.

The description presented in this paper for hydrogen-enhanced deformations of Pd during cathodic hydrogen charging and anodic discharging cycles, as well as the consistency of resulting data, reveals the relevance of nanoscopies to follow mechanical deformations of solids at the nanometer level, both in volume and surface, in real time, and discriminate the different types of deformations taking place simultaneously in solids.

Acknowledgment. This work was financially supported by PIA 7283/97, PIP 4379/97, and PIP 014/97 from the Consejo Nacional de Investigaciones Científicas y Técnicas (CONICET) of Argentina.

LA980633F